ECE

WEMPEC

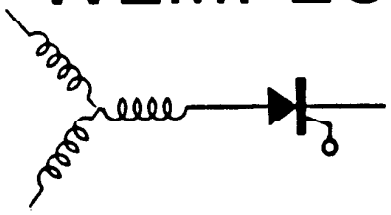

UNIVERSITY OF WISCONSIN MADISON

Wisconsin Electric Machines and Power Electronics Consortium

RESEARCH REPORT
85-3

Determination of Equivalent Circuits for Induction Machines with Skin Effect Using Terminal Characteristics

W. H. Creer, D. W. Novotny, T. A. Lipo
University of Wisconsin
Madison, Wisconsin

Department of Electrical and Computer Engineering
University of Wisconsin-Madison
Madison, Wisconsin 53706

March 1985

DETERMINATION OF EQUIVALENT CIRCUITS FOR INDUCTION MACHINES WITH SKIN EFFECT USING TERMINAL CHARACTERISTICS

W.H. CREER, Eaton Corporation,

D.W. NOVOTNY, University of Wisconsin-Madison, and

T.A. LIPO, University of Wisconsin-Madison

ABSTRACT

Extended equivalent circuits for modelling induction machines with rotor bar skin effect are developed using a method that relies on terminal frequency response characteristics rather than rotor bar dimensional data. Some experimental verification of the models is provided in addition to comparison of the steady state torque speed curves.

1. INTRODUCTION

Operation of induction machines during start-up, shock loading and steady state excitation with non-conventional sources is accompanied by transient air gap torques, harmonic losses and other frequency dependent behaviors for which the Stanley Equations are not adequate [1]. Proper handling of skin effect can lead to more accurate motor models and excellent results have been obtained by assuming that the rotor bars are composed of smaller subdivisions within each of which the current density is constant. Traditionally these schemes have used actual dimensional data from the rotor bar geometry [2]. Recent developments in standstill frequency response (SSFR) modelling of large synchronous generators, however, have employed techniques for circuit determination from curve fitting to actual measured frequency responses [3]. The latter concept has been employed here for the modelling of induction machines that have high frequency parameter sensitivity.

The initial motivation for the work reported in this paper was to enable more accurate modelling of rotor losses resulting from non-sinusoidal excitation, especially in the case of phase back voltage control [4,5]. Earlier work [5] demonstrated that a single secondary circuit model considerably underpredicted the motor losses with phase back control. One primary goal of the present work was to ascertain the extent to which this error was attributable to skin effect phenomena. In the course of the work other skin effect related questions, such as stalled torque characteristics, were also examined.

2. DEVELOPMENT OF THE MODEL

Four important assumptions employed in the development of the rotor model to account for skin effect are;

1) The cross section of each of the rotor bars can be considered as a composite of smaller subdivisions each covering a sufficiently small area so as to make the approximation of uniform current density within it accurate.

2) The air gap flux entirely links the rotor bar so as to equally excite all of the bar sections described above.

3) The subdivisions into which the rotor bar is divided all have equal cross sectional areas.

4) The subdivisions all have rectangular cross sectional geometry and are configured as a stack of conductors with either increasing or decreasing breadth so as to approximate a complete rotor bar geometry that is trapezoidal as shown in Fig. 1.

Condition 1 implies that each of the subdivisions can be modelled as a series R-L circuit with constant parameters similar to the rotor portion of the standard induction motor equivalent circuit, the difference being that it is not only magnetically coupled to the stator circuit but to the other rotor circuits as well. Condition 2 implies that the same excitation voltage is applied to each of the subdivisional circuits, thus resulting in the equivalent circuit form of Fig. 2.

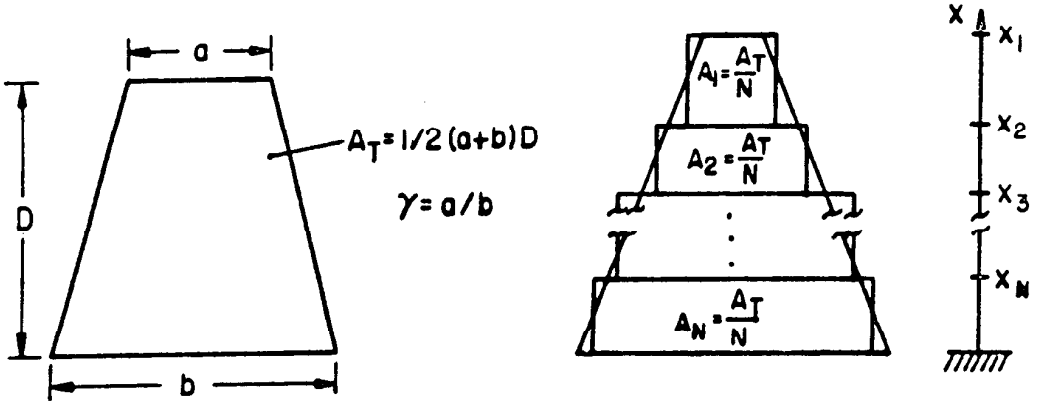

(i) (ii)

FIGURE 1: (i) Trapezoidal Conductor and,
(ii) Piecewise Rectangular Approximation

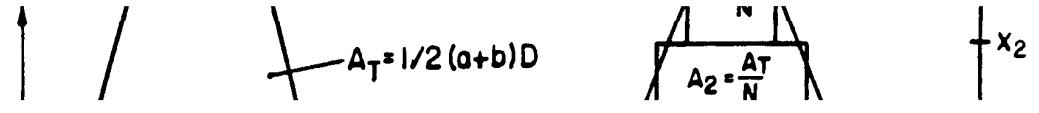

Since the cross sectional area of each of the subdivisions is equal to that of the others as specified by condition 3, all of the branch resistances of Fig. 2 are the same and are equal to N times the dc resistance of the complete conductor where N is the number of regions into which it is divided.

Finally, the breadth and depth of each of the subdivisional areas can be expressed as a function of two parameters related to the trapezoidal cross section that is to be geometrically approximated;

1) the total depth of the conductor, D, and
2) the ratio of the upper and lower bases of the trapezoid, $\gamma = a/b$.

The resistance of each leg of Fig. 1 can then be expressed as

$$R_i = (\rho/(A/\ell)) \quad i = 1,2,\ldots,N \tag{1}$$

where: A = the area of each subdivision
= (1/N) times the total cross sectional area
ℓ = the axial length of the conductor, and
ρ = the resistivity of the conductor material.

It can also be shown [6] that the self and mutual inductances of the conductor subdivisions are

$$L_{ii} = L_i + 3 \sum_{k=1}^{k=i-1} L_k \tag{2}$$

and

$$M_{ij} = M_{ji} = (3/2) L_i + 3 \sum_{k=1}^{k=i-1} L_k \quad j>i \tag{3}$$

where:

$$L_k = (1/3)(\mu_o/(A/\ell))(d_k)^2 \quad k = 1,2,\ldots,N \tag{4}$$

$$d_k = x_k - x_{k+1} \tag{5}$$

and where:

$$x_k/D = 0 \qquad k = N + 1 \tag{6a}$$

$$x_k/D = \frac{1 - \sqrt{1 - ((N - k + 1)/N)(1 - \gamma^2)}}{1 - \gamma} \qquad \gamma \neq 1 \tag{6b}$$

and

$$x_k/D = ((N - k + 1)/N) \qquad \gamma = 1 \tag{6c}$$

Eqs. (6b) and (6c) are valid for $k = 1,2,\ldots,N$.

Equations (1) through (6) allow the circuit of Fig. 1 to be reconfigured as that of Fig. 3 consisting only of resistances and magnetically uncoupled inductances.

If it is assumed that end ring leakage is negligibly small compared to slot leakage, or at least that it can be adequately accounted for elsewhere in the motor equivalent circuit, then Fig. 3 also represents the stator refered rotor equivalent since each component is simply multiplied by the (constant) square of an equivalent turns ratio in the referral process.

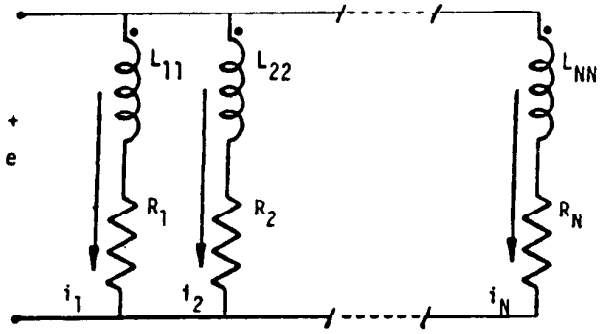

FIGURE 2: Equivalent Circuit of Bar Sections with Equal Excitation

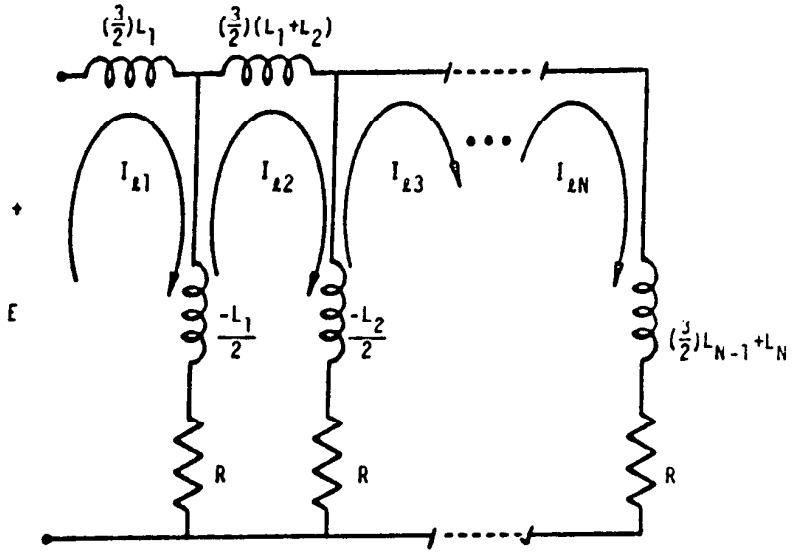

FIGURE 3: Ladder Equivalent of the Rotor Resulting from Condition 4

3. DETERMINATION OF THE EQUIVALENT CIRCUIT FOR AN INDUCTION MOTOR WITH KNOWN FREQUENCY RESPONSE

Frequency response data for the motor with nameplate data given in Appendix A was obtained from laboratory tests and is shown in Fig. 4. The stator and dc rotor resistances are known to be 0.023 pu and 0.0145 pu respectively. The core loss resistance and stator self reactance have been found [7] to be well approximated by the polynomials given by Eqs. (7) and (8).

$$R_m = 24.57(0.6186 + 0.4614\lambda + 1.3096\lambda^2 - 1.3317\lambda^3) \quad (7)$$

$$X_s = X_{\ell s} + X_m = 0.0145 + 1.4686(0.5922 + 4.7605\lambda - 12.6110\lambda^2 + 15.5361\lambda^3 - 8.1026\lambda^4 + 0.6711\lambda^5) \quad (8)$$

where: λ is the pu gap flux linkage

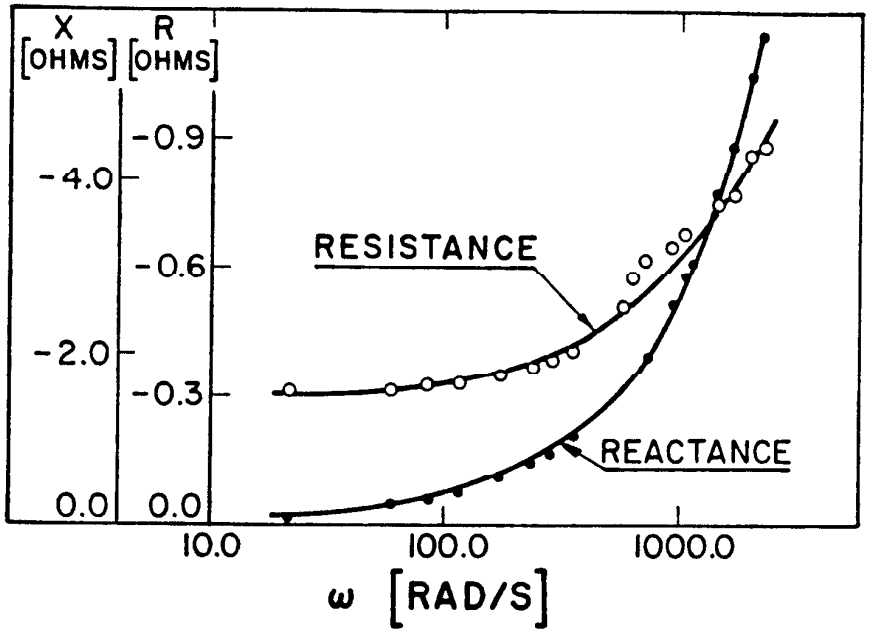

FIGURE 4: Measured Per Phase Impedance Frequency Response of the Motor Described in Appendix A

3.1 The Search Technique

The subdivisional time constants, T_k, can be defined as

$$T_k = L_k/R_k = (\mu_o/3N\rho)\, d_k^2 \quad (9)$$

For given values of stator and magnetization parameters the frequency response of the rotor circuit as seen by the air gap can be calculated from Fig. 4. A search over the plane defined by γ and D can then be implemented to find the geometric parameters providing the minimum model frequency response deviation from that of the actual data according to some acceptable error criterion. The error function used in this case is given by Eq. (10) and can be seen to accumulate weighted deviations of the resistance and the reactance.

$$E_R = (100/R_{DC} \cdot NDAT) \left(\sum_{j=1}^{j=NDAT} (1-\sigma)[R_M(\omega_j)-R_A(\omega_j)]^2 + (\sigma)[X_M(\omega_j)-X_A(\omega_j)]^2 \right)^{0.5} \qquad (10)$$

NDAT is a measure of the frequency range of the model and the subscripts M and A identify values for the model and actual responses respectively.

3.2 Treatment of Stator Leakage

Note that since it is the stator self reactance that can be measured from synchronous speed tests some freedom is allowed in the designation of stator leakage inductance. Thus, a good procedure for determination of the extended equivalent circuit is as follows. First, a particular value of stator leakage inductance is assumed and the air gap frequency response calculated. Then the search outlined above is implemented to find the best γ and D for the assumed value. This should then be repeated for various values of leakage inductance until the best combination of the three parameters, $L_{\ell s}$, γ and D, is found. Finally, γ and D are used in Eq. (9) to complete the equivalent circuit.

3.3 Equivalent Circuit Results

For a 3 branch rotor equivalent circuit of the motor described in appendix A with an upper limit of 400 Hz for the frequency response, the best fit parameters were found to be

$L_{\ell s}$ = 1.9 mH
γ = 0.168
D = 1.482 cm

which provided an error of E_R = 0.645.

For the less demanding fit to an upper frequency limit of only 60 Hz the best fit parameters were found to be

$L_{\ell s}$ = 2.1 mH
γ = 1.677
D = 1.947 cm

which provided an error of E_R = 0.130.

The air gap frequency responses of the two cases are shown in Figs. 5 and 6 and the equivalent circuits are shown in Figs. 7 and 8 respectively.

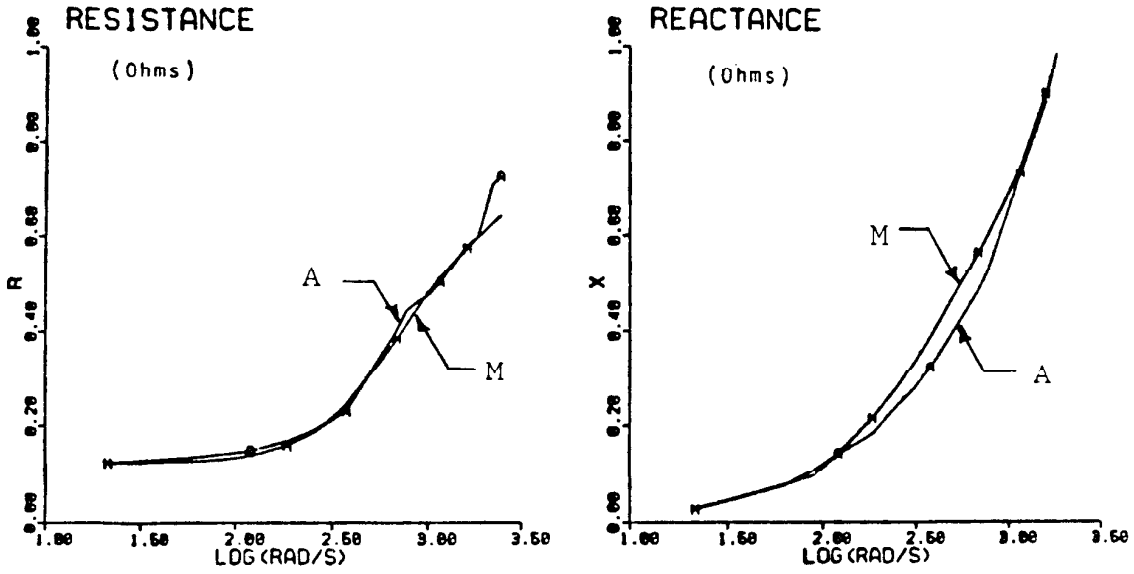

FIGURE 5: Actual (A) and Model (M) Rotor Impedence Frequency Responses for a Limit Frequency of 400 Hz

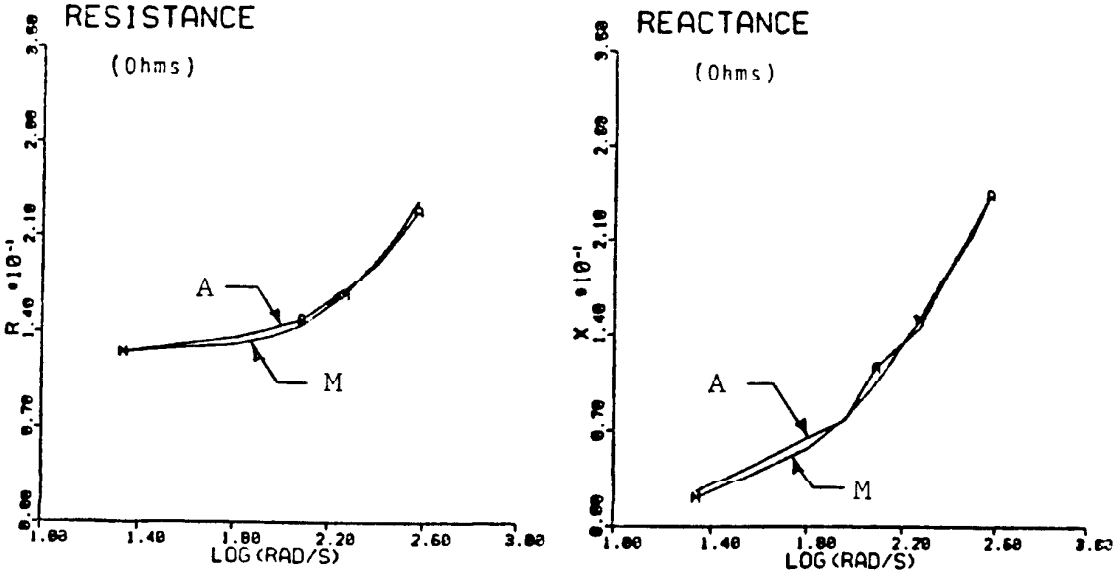

FIGURE 6: Actual (A) and Model (M) Rotor Impedence Frequency Responses for a Limit Frequency of 60 Hz

Notice that a better fit was found for the second case. This is to be expected since the frequency range to which the model was fitted comprises a much narrower band. A better fit for the 400 Hz case could be easily found by using more subdivisions of the rotor bars. This would have the disadvantage, of course, of resulting in a higher order model.

$$X_s = X_{\ell s} + X_m = 0.1045 + 1.4686(0.5922 + 4.7605\lambda - 12.6110\lambda^2 + 15.5361\lambda^3 - 8.1026\lambda^4 + 0.6711\lambda^5)$$

$$R_m = 24.57(0.5186 + 0.4615\lambda + 1.3096\lambda^2 - 1.3317\lambda^3)$$

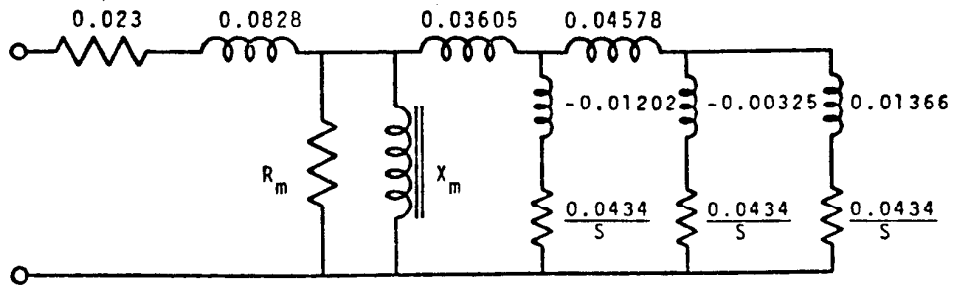

FIGURE 7: Per Unit Steady State Equivalent Circuit Corresponding to the Model of Figure 5
$X_m = X_s - 0.0828$

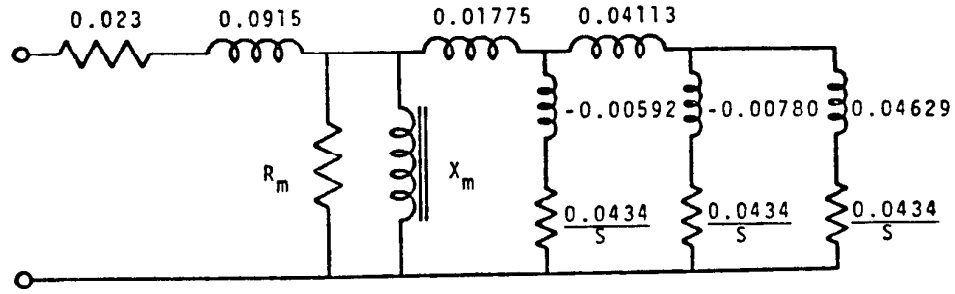

FIGURE 8: Per Unit Steady State Equivalent Circuit Corresponding to the Model of Figure 6
$X_m = X_s - 0.0915$

3.4 Comparison of Models

A phase back type SCR voltage regulator was used to drive the motor at a condition slightly over 1/4 load in order to evaluate the performance of the extended models. A schematic outline of the test set-up is shown in Fig. 9 and the typically harmonic rich waveforms produced by the regulator are shown in Fig. 10. Measured electrical values were compared to the corresponding values predicted by the various motor models. For the given load condition the following values were measured

γ_h = 31.5 degrees
S = 0.0052
P_m = 0.313 pu
I_s = 0.727 pu

A digital oscilloscope was used to record the waveforms and a point by point integration was employed to determine the motor input power P_m, and the rms stator current I_s.

The three models, single branch standard, three branch low frequency and three branch high frequency were used to obtain predictions of the power and current for the specified (measured) values of hold-off angle γ_h, and slip S. The results of all three models are given in Table 1 as percent deviations from the measured values.

Since skin effect is a second order characteristic it is difficult to obtain data accurate enough to display its influence. To do so requires some method of accounting for other second order effects exhibited by the system. In particular, the tendency of the bar resistance to rise with frequency requires some accommodation for the behavior of the resistance with respect to temperature. Therefore, additional entries have been provided in Table 1 for coarse adjustments of the motor resistances for temperature effects. The cold values were measured at room temperature (near 20 °C). The hot values are for 5, 10 and 15 percent increases over the cold values, roughly corresponding to conductor temperatures of 30 °C, 45 °C and 60 °C respectively.

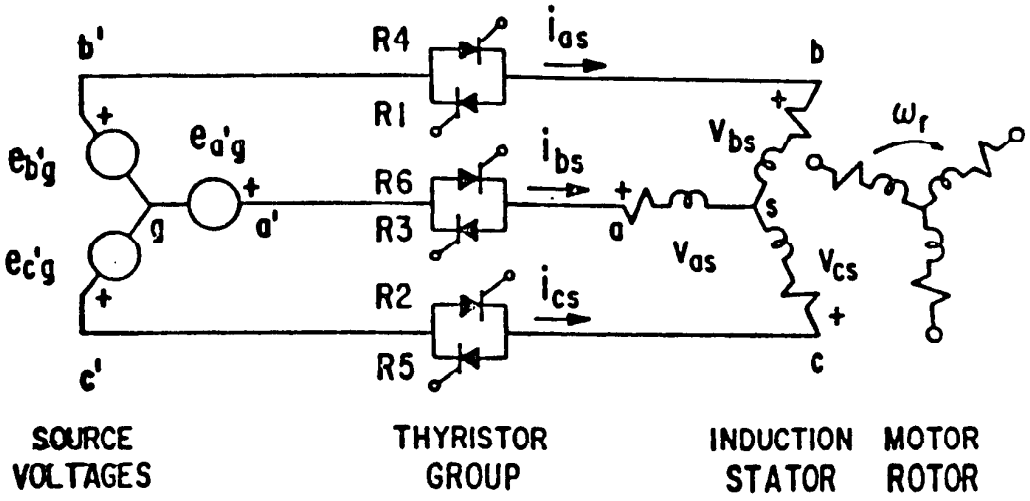

FIGURE 9: Induction Motor with Phase Back Type Voltage Controller

It can be observed that the three branch models provided good predictions of the current with and without adjustment for the temperature effect while the standard model underpredicted this value. It can be noted however, that with no temperature adjustment the three loop model overpredicted the input power and the standard model was quite accurate. But with reasonable temperature adjustments the overall precision of the three loop models improved while that of the standard model declined.

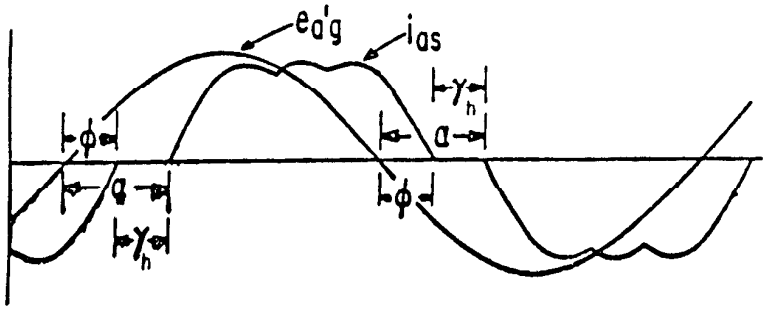

FIGURE 10: Typical a - Phase Waveforms for the circuit of Figure 9

TABLE 1: Power and RMS Stator Current of the Models as Percent Deviations from the Measured Values

$\gamma_h = 31.54^{\circ}$ S = 0.00521 Voltage = 1.06 pu

RESISTANCE ADJUSTMENT FOR TEMPERATURE EFFECTS

	STANDARD		3 LOOP 60 Hz		3 LOOP 400 Hz	
	ΔP_m	ΔI_s	ΔP_m	ΔI_s	ΔP_m	ΔI_s
NONE	+2.42 %	-8.06 %	+13.00 %	+1.60 %	+13.90 %	+1.98 %
+ 5 %	-1.69 %	-9.28 %	+9.22 %	-0.13 %	+9.55 %	+0.79 %
+ 10 %	-5.41 %	-10.09 %	+5.10 %	-1.13 %	+5.53 %	-0.29 %
+ 15 %	-8.79 %	-11.25 %	+1.09 %	-2.09 %	+1.75 %	-1.24 %

4. APPLICATION TO MOTORS WITHOUT KNOWN FREQUENCY RESPONSE

For the circumstance in which no frequency response information about the motor is known but a standard form equivalent circuit is available, two additional assumptions can make rather coarse evaluations of skin effect characteristics possible. They are;

1) The rotor leakage inductance and rotor resistance of the standard model are known as a result of tests at sufficiently low frequency as to make them very nearly equal to the dc values, and

2) The true frequency response of the rotor conductors can be adequately approximated by the calculated [8] response of rectangular bars.

4.1 Method of Application and Specific Results

The frequency response of a rectangular bar was calculated according to Alger [8] and the search described in Section 3 (without adjustment of $L_{\ell s}$, of course, which has no meaning in this case) was applied to find the best fit parameters for the subdivided trapezoidal approximation. The best fits were found for 3 and 5 section bars as a function of $\omega_L T_{\ell r}$ where ω_L is the limit frequency of the model and where $T_{\ell r}$ is the rotor leakage

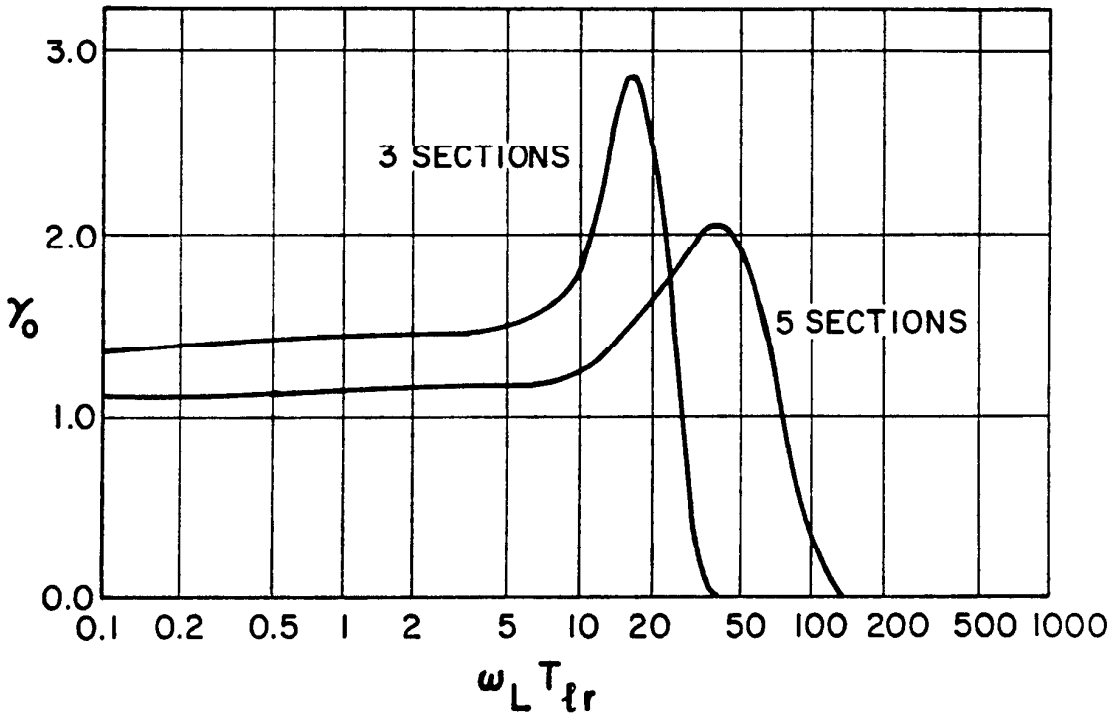

FIGURE 11: Best Fit Shape Factor γ_o for 3 and 5 Section Models of a Rectangular Conductor

time constant of the given standard motor model. The best fit shape factor and depth are shown in Figs. 11 and 12 respectively. Note that the depth of Fig. 12 is normalized to d, the true depth of the rectangular conductor from which the frequency response was calculated so as to make the curves applicable to rectangular conductors in general. The curves were found for a constant weighting factor of $\sigma = 0.5$ and the resulting error, also a function of $\omega_L T_{\ell r}$, is shown in Fig. 13.

The rotor leakage time constant is given by

$$T_{\ell r} = L_{\ell r}/R_r = (\mu_o/3\rho)\, d^2 \qquad (11)$$

and the individual time constants of the subdivisions are defined as

$$T_k = L_k/R_k = (1/N)\, L_k/R_{DC} \qquad k = 1,2,\ldots,N \qquad (12)$$

which can be put into a form similar to (11)

$$T_k = (\mu_o/3N\rho)\, d_k^2 \qquad (13)$$

Equation (13) reduces to

$$T_k = (T_{\ell r}/N)(D_o/d)^2[(X_k/D_o) - (X_{k+1}/D_o)]^2 \qquad (14)$$

where X_k/D_o and X_{k+1}/D_o are defined by Fig. 1 and are quantified by Eq. (6).

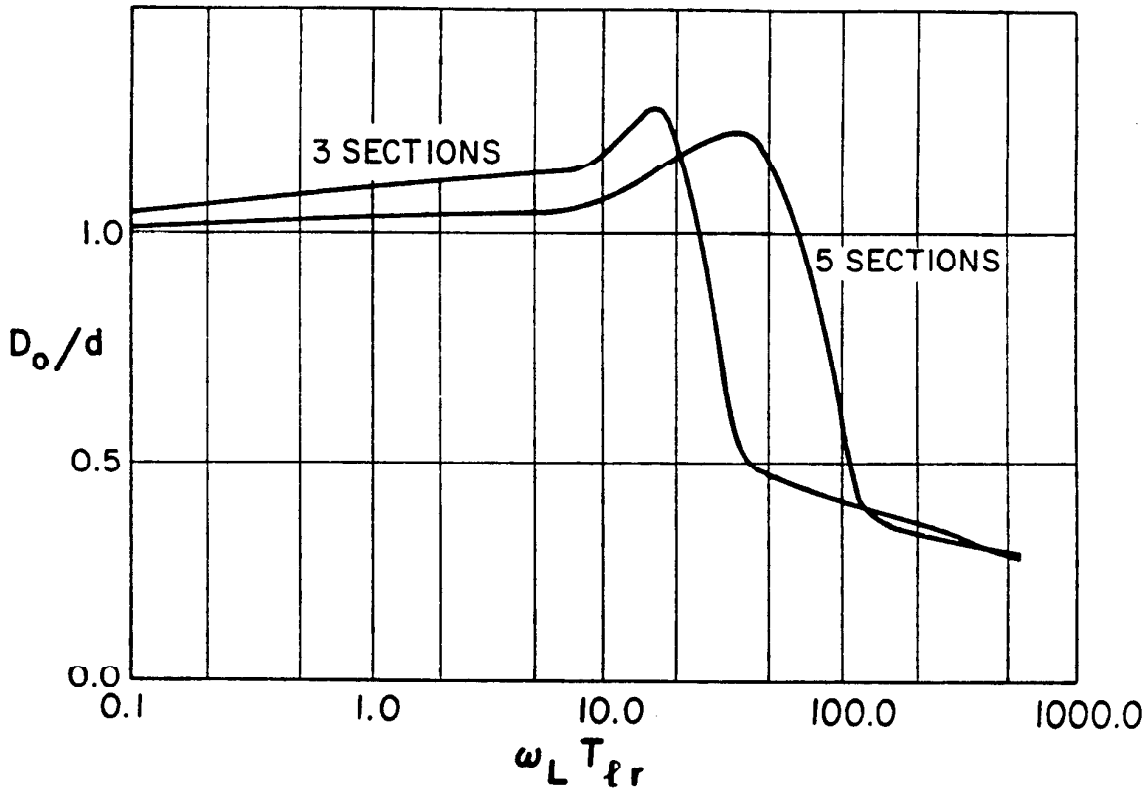

FIGURE 12: Best Fit Depth Ratio D_o/d for 3 and 5 Section Models of a Rectangular Conductor

Thus for a given $L_{\ell r}$ and R_r, $T_{\ell r}$ can be found from (11) and if a limit frequency for the extended model is specified $\omega_L T_{\ell r}$ can be used to find γ_o and D_o/d from Figs. 11 and 12. Finally, the T_i's can be found from (14) and the L_i's from (12).

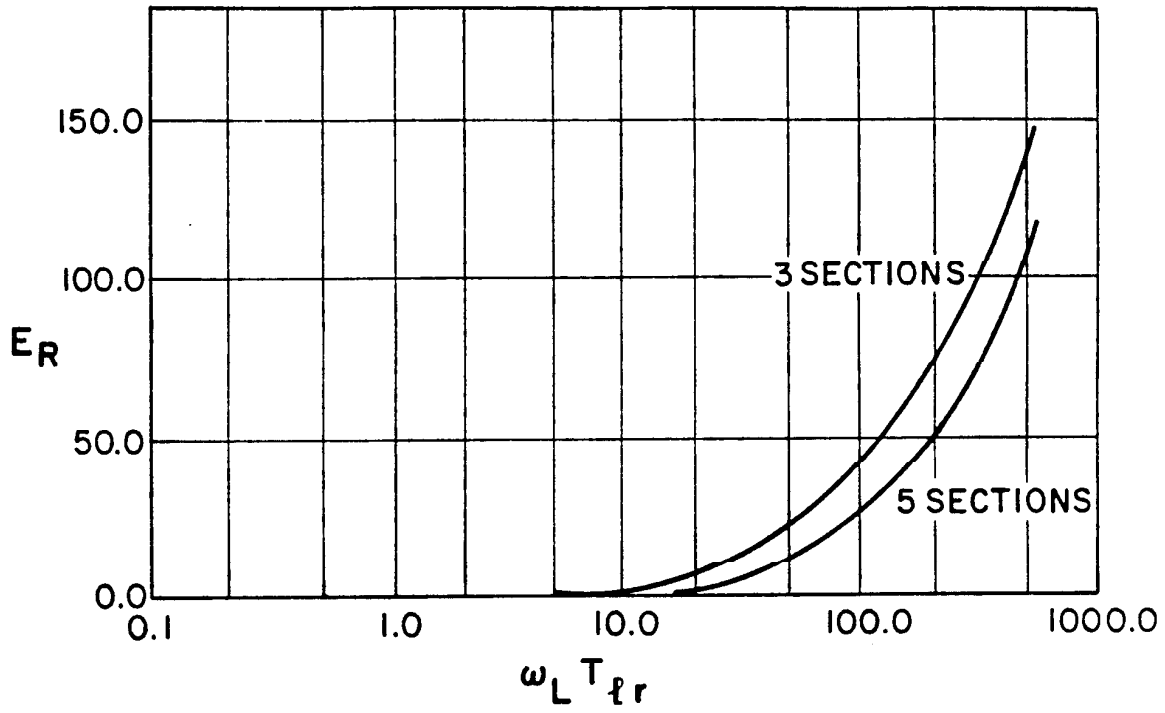

FIGURE 13: Errors for the Best Fit 3 and 5 Section Models of a Rectangular Bar

4.2 Comparison of Models

Figure 14 shows a standard induction motor equivalent circuit in per unit form for a low horsepower induction motor. The method described above was applied twice to find two three-branch equivalents for limit frequencies of 60 and 500 Hz. The resulting circuits are shown in Figs. 15 and 16. Note that for the 500 Hz limit frequency the error found from Fig. 13 is quite substantial but could be reduced by forming a model with more branches.

The three models were used to obtain steady state torque speed curves with one per unit stator voltage and the results are shown in Fig. 17. Note that for very low values of slip the performance characteristics of all three models are nearly identical. This is to be expected since the rotor frequency imposed near synchronous speed is very low and obscures the skin effect characteristics. For speed near and below breakdown however, the characteristics of the three model are substantially different.

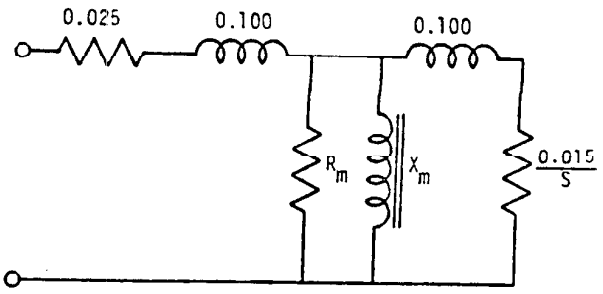

FIGURE 14: Standard Equivalent Circuit of a Typical Induction Motor

$$R_m = 14.14 + 15.64\lambda + 19.13\lambda^2 - 20.40\lambda^3$$

$$X_m = 0.87 + 7.61\lambda - 20.54\lambda^2 + 27.15\lambda^3 - 17.14\lambda^4 + 3.66\lambda^5$$

Values are in Per Unit Form

Comparison of the characteristics of the standard model and the 60 Hz three branch model are encouraging as evidence of the ability of the extended model to better represent the motor for high slip conditions with sinusoidal excitation. The locked rotor torque predicted by the standard equivalent is much lower than can be accepted as representative of a real motor while that of the 60 Hz three branch model is much closer to the NEMA standards.

Figure 17 also shows the characteristics of the 500 Hz three branch model. It can be expected to provide a better approximation (but not necessarily a satisfactory one) to the true response of the machine to harmonic excitation than either of the other two models. It also provides an acceptable representation of the motor for fundamental excitation as long as the slip remains sufficiently below that at which breakdown occurs. Caution should be exercised in using this model for fundamental component computations near breakdown since it gives substantially higher torques than can be expected of the actual motor.

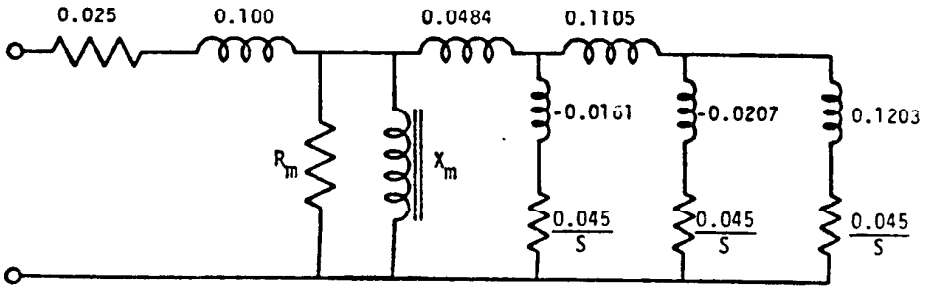

FIGURE 15: Extension of Figure 14 to a 3 Section Model with a Limit Frequency of 60 Hz

5. SUMMARY

Conductors with non-uniform current distributions have been modelled as multiple conductor sections each with uniform current density. Parameters for the extended equivalent circuits have been determined from motor frequency response characteristics and the assumption of a trapezoidal rotor bar cross section.

Extended models have been used to predict input power and current to a motor supplied with harmonic rich excitation and the results provide encouragement for continued invesigation of this method of accounting for the deep bar effect. In addition, curves describing the geometrical parameters of 3 and 5 section models for bars with rectangular cross sections have been provided, and the steady state torque-speed characteristics of these models have been shown to compare favorably to those of the standard, single secondary circuit induction motor model.

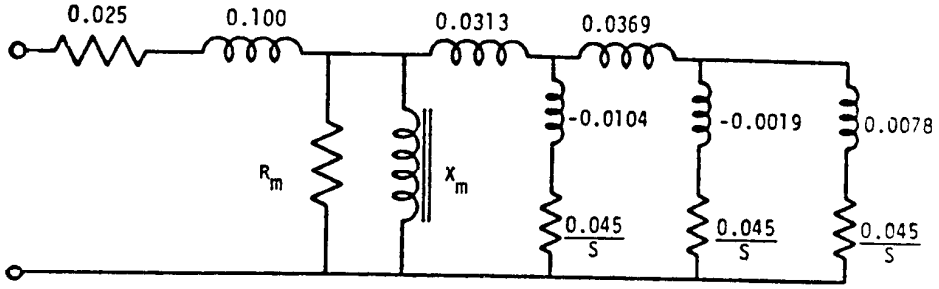

FIGURE 16: Extension of Figure 14 to a 3 Section Model with a Limit Frequency of 500 Hz

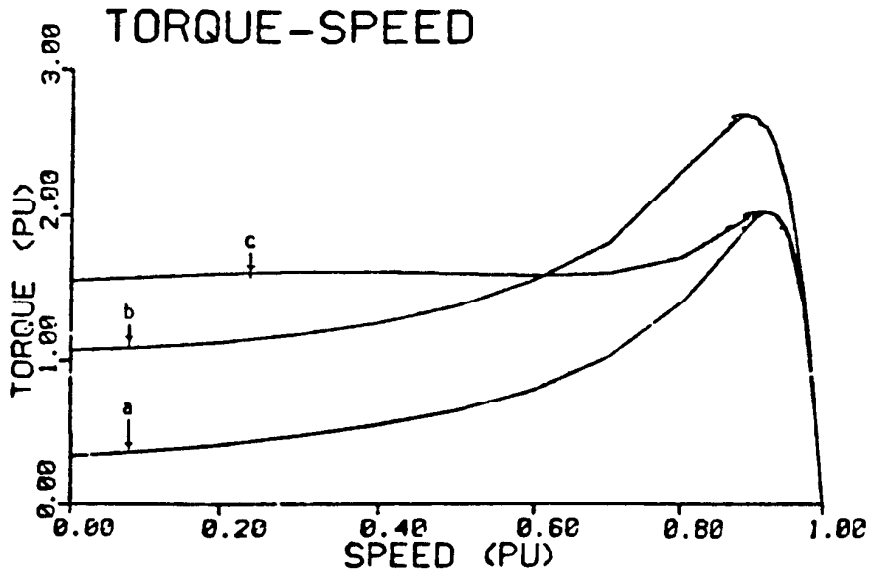

FIGURE 17: Steady State Torque - Speed Curves for;
a) the Standard Model,
b) the 3 Section 500 Hz Model and
c) the 3 Section 60 Hz Model

Suggestions for future work include modelling of different cross sectional geometries and a study of the weighting factor used in the error criterion (10). The weighting factor may possibly be best represented as a function of frequency (σ_i) so as to prevent the reactance from dominating at high frequencies. It would also be interesting to determine proper use of the weighting factor for specific model applications. That is, values of σ that are appropriate for harmonic loss studies may be distinct from those that are appropriate for a study of starting and braking torques.

REFERENCES

1. R.F. Smith and J.O. Nichols,"Analysis of a Deep Bar Induction Motor and Compressor Load During Start-Up," IEEE Trans. on Power Apparatus and Sys., Vol. PAS-97, No. 5, September/October 1978, pp. 1696-1705.

2. E.A. Klingshirn and H.E. Jordan,"Simulation of Polyphase Induction Machines with Deep Rotor Bars," IEEE Trans. on Power Apparatus and Sys., Vol. PAS-89, No. 6, July/August 1970, pp. 1038-1043.

3. J.D. Hurley and H.R. Schwenk,"Standstill Frequency Response Modelling and Evaluation by Field Tests on a 645 MVA Turbine Generator," IEEE Trans. on Power Apparatus and Sys., Vol. PAS-100, No. 2, February 1981, pp. 828-836.

4. T.A. Lipo,"The Analysis of Induction Motor Voltage Control by Symmetrically Triggered Thyristors," IEEE Trans. on Power Apparatus and Sys., Vol. PAS-90, No. 2, March/April 1971, pp. 515-525.

5. T.M. Rowan,"Quantitative Analysis of Induction Motor Performance Improvement by SCR Voltage Control," M.S. Thesis, University of Wisconsin-Madison, 1982

6. W.H. Creer,"Modelling Deep Bar Effects in Induction Machines," M.S. Thesis, University of Wisconsin-Madison, 1984.

7. D. Kirschen,D.W. Novotny and W. Suwanisoot,"Minimizing Induction Motor Losses by Excitation Control in Variable Frequency Drives," IEEE Trans. on Ind. Appl., Vol. IA-20, No. 5, September/October 1984, pp. 1244-1250.

8. P.L. Alger,"Induction Machines," Second Edition, (book) Gordon and Breach Science Publishers, New York, New York, 1970.

APPENDIX A

Nameplate Data: Baldor Electric Co.
7.5 Hp, Frame 924M 284T, 208/220/440 volts
21/20/10 Amps 60 Hz

Per Unit Parameters: $R_s = 0.023$ $R_r = 0.014$

$X_{\ell s} = X_{\ell r} = 0.1045$ $R_m = 21.0$ $X_m = 1.4$ (nominal)